Effect of gold nanoparticles (AuNPs) on isolated rat tracheal segments

Daniel Alberto Maldonado-Ortega [a,1], Gabriela Navarro-Tovar [a,b,c,1], Gabriel Martínez-Castañón [d], Carmen Gonzalez [a,b,*]

[a] Facultad de Ciencias Quimicas, Universidad Autonoma de San Luis Potosi, Manuel Nava 6, Zona Universitaria, 78210, San Luis Potosi, SLP, Mexico
[b] Centro de Investigacion en Ciencias de la Salud y Biomedicina, Universidad Autónoma de San Luis Potosi, Sierra Leona 550, Lomas de San Luis, 78210, San Luis Potosi, SLP, Mexico
[c] Consejo Nacional de Ciencia y Tecnologia, Insurgentes Sur 1582, Crédito Constructor, Benito Juárez, 03940, México City, Mexico
[d] Facultad de Ciencias, Universidad Autonoma de San Luis Potosi, Parque Chapultepec 1570, 78210, San Luis Potosi, SLP, Mexico

ARTICLE INFO

ABSTRACT

The AuNPs have been used in biomedicine as therapeutic tools for cancer. However, its role in the context of respiratory physiology has been little studied. This study aimed to determine the impact of AuNPs on respiratory smooth muscle tone, using a model of isolated tracheal rings from female and male rats precontracted with acetylcholine (ACh). AuNPs exerted a contractile effect only in the concentration of 100 ug/ml. This contractile effect was not modified by gender. The possible mediator $^{+}$could be nitric oxide (NO), measured in a physiological solution containing the tracheal rings treated with different concentrations of AuNPs. The results obtained in this study show that the AuNPs are bio-inert in a concentration range of $0.1-10$ μg/mL; however, 100 μg/mL could trigger airway hyperresponsiveness. Similar effects were obtained in isolated trachea rings treated with 100 μg/mL HAuCl4. An evaluation of HAuCl4 in physiological buffer at various HEPES concentrations (0–20 mM) showed the formation of AuNPs that could explain the contractile effect on the tracheal smooth muscle.

1. Introduction

Nanotechnology includes metallic nanoparticles as structures with at least one of their dimensions within the nanoscale range ($1-100$ nm), with unique properties that differ from bulk materials (Chen & Schluesener, 2007). Among metallic nanoparticles are the gold nanoparticles (AuNPs) that, by their nature and intrinsic properties, such as optoelectronic and sizeable surface-area-to-volume ratio, have been proposed as an excellent material for biomedical applications [1].

AuNPs have been historically used in stained glass and lusterware pottery art to confer wine red color. In this context, AuNPs found in red glasses dated back to the Late Bronze Age and art pieces like the famous Roman Lycurgus Cup dated from the 4th century [2]. The first description of gold nanoparticles was attributed to Michael Faraday (1857), who discussed the ruby color of colloidal gold obtained from a gold salt and citric acid reaction. About 100 years later, Turkevich et al. reported that particles of 6 nm were responsible for the ruby color of colloidal gold [3]. Besides Turkevich's methods, other chemical

methods are available to obtain AuNPs, such as synthesis with NaBH4, Brust-Schiffrin method, seeding-growth method, various green synthesis methods, among others [4]. Current studies with AuNPs from 10 to 100 nm consider the use of colloidal nanospheres [5], non-spherical AuNPs [6], nanohybrids with silica-coated Au nanoshells, polymer-Au nanohybrids [7], and chitosan-Au complexes [8]. In the last decade, AuNPs-based nanomaterials have demonstrated their potential as 1) drug delivery vehicles for antitumoral [9–12], antimicrobial [13–15], and analgesic molecules [16–18], as well as DNA [19–21], peptides and proteins [22–25], 2,) as constituents of scaffolds in tissue engineering [26,27], 3) as biosensor [28–30], 4) for the thermal ablation therapy of solid tumors [31–33], and 5) imaging and theragnostic devices [34,35].

However, the nanotoxicology of AuNPs remains controversial since various parameters (particle size, concentration, chemistry onto the particle surface, functionalization molecules, time of exposure) are involved in the overall effect on biological systems, and evaluations conducted in cell cultures, isolated organs, and animal models. For instance, AuNPs of ~10 nm induce a toxic effect in healthy cell cultures

causing impairment of lysosome degradation in rat kidney (NRK) cells [36], but no considerable effects on the cell viability when human dermal microvascular endothelial cells and human cerebral microvascular endothelial cells treated with AuNPs with the same size and surface charge [37]. Moreover, surface chemistry variations result in different effects on cell cultures. [38] demonstrated in glioma U87 cell and fibroblast cells treated with 100 µg/mL AuNPs with 25 nm of diameter with cetyl trimethyl ammonium bromide (CTAB), polyethyleneglycol (PEG), or human serum albumin, being CTAB the most toxic component and PEG the less toxic. On the other hand, 5 and 30 nm AuNPs coated with PEG showed relatively low toxicity in male mice (intraperitoneal administration of 4000 µg/kg), while 60 nm AuNPs with the same coating induce severe damage to the liver and kidney [39]. Other *in vivo* models showed no evidence of atrophy, hyperplasia, or inflammation in any organ of nude female mice (Athymic Nude-Foxn1nu) treated with a single dose (1 mg/kg) of 21 nm dextran-coated AuNPs [40]. Thus, contradictory evidence and the use of different biomodels clarify the need for systematic evaluation of novel nanomaterials, such as AuNPs and AuNPs-hybrids.

In this respect, physiological models of isolated organs could generate accurate information in real-time regarding nanomaterials' impact on tissues and cells and establish a safe range of nanomaterial concentration. The isolation of the lung, liver, aorta, heart, intestine, among other organs, maintains the focus on nanoparticles mechanism of action in a target system since alterations in the organ (contraction, relaxation, changes in biomarker levels) can be measured within few hours. Later, the tissues can be processed for histopathologic studies. Notably, few studies in aorta smooth muscle cavities such as isolated aortic and trachea rings have been conducted to determine the metallic nanoparticles biosafety. Holland et al. [41] isolated coronary artery and aorta vessel segments from Sprague Dawley rats previously exposed to 200 µg (oral administration) of either 20 or 110 on gold core silver nanoparticles covered with a cationic polyvinylpyrrolidone (PVP) polymer. The stimuli with phenylephrine (Phe) and serotonin (constrictor agents), and ACh (vasodilator agent) showed that aortic rings exhibited impaired endothelial independent NO relaxation seven days after exposure [41]. Alkilany et al. [42] also reported the strong relation between surface chemistry and nanoparticle toxicity in aortic rings isolated from male Wistar rats exposed to gold nanorods modified with either polyelectrolyte-CTAB or thiolated PEG. Thiolated capped gold nanorods did not alter the aortic function (biocompatible), while polyelectrolyte-CBAT capped gold nanoparticles decreased NO production and impaired endothelium-dependent relaxation (toxic effect) [42]. To our knowledge, no evaluations of AuNPs have been reported in isolated rings of the trachea. However, our research group has determined the impact of other metallic nanoparticles, such as the 45 nm silver nanoparticles (AgNPs) in the trachea, in which contractile effect was observed and associated with the alteration of acetylcholine muscarin receptor and increasing on the production of NO [43,44], suggesting that AgNPs (0.1–100 µg/mL) could sensitize the trachea.

Thus, this study aimed to determine the effect of AuNPs as regulators of tracheal smooth muscle tone, using a model of isolated rings of male and female rat trachea.

2. Methodology

2.1. Synthesis and characterization of AuNPs

AuNPs synthesized as described by Moreno-Alvarez et al. [45]. Briefly, solutions of 0.001 M gold (III) (HAuCl₄•3H₂O; Sigma-Aldrich, St. Louis, MO, USA) and 0.001 mol of gallic acid (Sigma-Aldrich, St. Louis, MO, USA) were prepared with deionized water. Then, 100 mL of gold (III) solutions and 10 mL of the gallic acid solution were placed into a flask under magnetic stirring and ambient temperature, adjusting pH to 10 using a basic solution of 1.0 M NaOH. The reaction was monitored by UV–vis spectroscopy (Ocean Optics S2000 UV–vis fiber optic

spectrometer) following the development of the golf nanoparticle plasmon. The gallic acid solution attachment was compared with a UV–vis spectrum obtained after the centrifugation of the sample's dispersion. A decrease in the absorption of gallic acid peak (262 nm) confirmed the molecule's adsorption onto the AuNPs surface [45].

2.2. Transmission electron microscopy analysis

AuNPs obtained were characterized using transmission electron microscopy (TEM) JEM -1230 (JEOL company, Peabody, MA) at an acceleration voltage of 100 kV. Physical characterization of synthesized AuNPs was performed by transmission electron microscopy (TEM) using JEM -1230 (JEOL company, Peabody, MA) instrument working at an accelerating voltage of 100 kV. Samples for TEM were deposited as suspensión in water onto carbon-coated grids. Images obtained were used to determine the average particle diameter using ImageJ software (Version 1.50, National Institutes of Health, Bethesda MD, USA), where over 100 particles in random view fields were counted.

2.3. Dynamic light scattering analysis

The hydrodynamic diameter and potential (ZP) of AuNPs were determined by dynamic light scattering (DLS) in a Malvern Zetasizer NanoZS (Instruments Worcestershire, United Kingdom). The equipment operated with a He-Ne laser, the wavelength was set at 633 nm, the detection angle at 90 degrees, and temperature at 25 °C. The lapse of the sample's analysis was 60 s.

2.4. Dispersion of AuNPs for physiological evaluations

A stock (197 µg/mL) of AuNPs previously characterized (diameter 11.6 nm $\pm$ 2.82) was dispersed by sonication (Sincor, Model Number SC-50TH) and stirred for 10 min to obtain a homogeneous suspension. Then, various AuNPs concentrations (0.1, 1.0, 10, and 100 µg/mL) were prepared for the physiological evaluation in trachea rings isolated from rats.

2.5. Evaluation of AuNPs-induced smooth muscle tone in isolated rat trachea

According to Rosas Hernández et al., 2009, muscle tone was evaluated using a model of isolated tissue from male and female rat trachea of the Wistar strain (300−350 g). The rats were anesthetized with an intraperitoneal sodium pentobarbital administration (50 mg/kg) and heparin (500 U). Later, the trachea was quickly removed, placed in physiological solution, and sectioned into 3–4 mm segments. Subsequently, the rings contained in physiological solution at a pH of 7.4 and 37 °C were coupled to isometric transducers and equilibrated for one hour [46]. The physiological solution contained NaCl 118 mM (Sigma-Chemical Company. St. Louis, MO, USA), KCl 4.6 mM, CaCl₂ 1.75 mM (Sigma-Chemical Company. St. Louis, MO, USA), MgSO₄ 1.2 mM (Sigma-Chemical Company. St. Louis, MO, USA), KH₂PO₄ 1.2 mM (Sigma-Chemical Company. St. Louis, MO, USA), dextrose (Sigma-Chemical Company. St. Louis, MO, USA) 10 mM, indomethacin (Sigma-Chemical Company. St. Louis, MO, USA) 3 µM and (4-2-hydroxyethyl)-1-piperazineethanesulfonic acid (HEPES) (Sigma-Chemical Company. St. Louis, MO, USA) 20 mM. Once stabilization was achieved, the rings were precontracted with 10 µM ACh, and subsequently, different single and/or cumulative concentrations of either HAuCl₄ (ionization control) or AuNPs (0.1, 1.0, 10 and 100 µg/mL) were administrated. The data obtained were collected in real-time and analyzed in the Polyview Data Acquisition and Analysis System software (Astro-Med, Inc Grass Instrument Division, West Warwick, RI). The use of animals was according to Ethical Protocols, CEID2014033, and CEID202003 approved evaluations.

2.6. Quantification of NO production

The production of NO was indirectly quantified through the formation of NO2/NO3 by the Griess method. Measurements were conducted in samples (500 μL) of a physiological solution containing the tracheal rings under the various treatments. Thus, the incubation time was fixed to 1 h at 37 °C in the presence of sulfonyl amide and N-(1-naphthyl)-ethylenediamine (Sigma-Chemical Company. St. Louis, MO, USA). Subsequently, the absorbance was quantified in a Bio-Rad microplate spectrophotometer (Hercules, CA, USA) at a wavelength of 490 nm, and the readings were interpolated in a calibration curve to calculate the concentration of NO_2/NO_3 (Rosas Hernández et al., 2009).

2.7. Analysis of data

Data were reported as the mean ± standard error of three independent experiments and analyzed by ANOVA using GraphPad Prism 5 software, with a confidence level of $P < 0.05$ or < 0.001.

3. Results and discussion

3.1. AuNPs are spherical and stable particles

DLS and TEM analysis revealed that spherical AuNPs have a slightly narrow size distribution with a mean particle size of 11.6 nm ± 2.82 (8.82 nm–14.46 nm) (Fig. 1A). The determination of hydrodynamic diameter (13.5 nm) indicated a monodisperse colloid (Fig. 1B), while zeta potential analysis determined a mean surface charge of -23.5 mV.

3.2. Contractile effect of AuNPs is concentration-dependent, but gender independent, and NO is involved in its mechanism

Treatments with cumulative concentrations (0.1, 1, 10 and 100 μg/mL) of $HAuCl_4$ showed that only those corresponding to 10 and 100 μg/mL exerted a contractile effect in trachea rings isolated from male rate, precontracted with 10 μM ACh (Fig. 2A), while in the treatments with cumulative concentrations of AuNPs, only the concentration of 100 μg/mL triggers a transient contraction (Fig. 2B). Furthermore, a differential effect was found for ACh contraction at the end of the respective treatments. For instance, $HAuCl_4$ limited the transient contractile effect exhibited by the second administration of 10 μM ACh (Fig. 2A). However, the AuNPs did not block this agent's second administration after administering the AuNPs, although the magnitude of the contractile

effects was less than that observed in the first administration before the treatment with AuNPs (Fig. 2B). In contrast, the treatments with 10 and 100 μg/mL of $HAuCl_4$ displayed a contractile effect of 52 and 65 %, respectively, while lesser effects were observed at 100 μg/mL AuNPs, being the contractile impact less than 40 % (Fig. 3A). A possible mediator of these contractile actions could be NO, since, in the treatments carried out with both $HAuCl_4 \bullet 3H_2O$ and AuNPs, it was observed an increment in the NO production (higher than 100 μM) at concentrations of 100 μg/mL (Fig. 3B). Similarly, data obtained in precontracted trachea rings isolated from female rats, where treatments with cumulative concentrations of $HAuCl_4 \bullet 3H_2O$ in a range of 10 and 100 μg/mL showed a contractile effect (Fig. 4A). In comparison, the cumulative administration of AuNPs exerted contraction at 100 μg/mL (Fig. 4B). When the concentrations of 10 and 100 μg/mL of $HAuCl_4 \bullet 3H_2O$ displayed again a contractile effect of 55 % and 65 %, respectively (Fig. 5A). Moreover, the contractile effect of AuNPs treatments was less evident at 100 μg/mL, being the highest percentage of contraction of 40 % (Fig. 5B). These findings could also be associated with an increment in the NO levels since treatments with both $HAuCl_4 \bullet 3H_2O$ and AuNPs at 100 μg/mL resulted in significant differences in controls (260 and 265 μM, respectively).

Other authors have described the correlation between the contractile effect on smooth muscle and NO production. Holland et al. [41] orally administrated 200 μg of 20 and 100 nm of gold core and silver-PVP to Sprague Dawley rats. The animals were sacrificed 1–7 days after treatment, and trachea rings were isolated and precontracted with Phe and serotonin. The authors described that impaired endothelial independent NO-dependent relaxation seven days after exposure [41]. Contrary, Silva et al. [47] found out that isolated aorta ring from male Wistar rats treated with 10 nm spherical AuNPs (0.3 nmol/L to 10 μmol/L) reduced the NO release but did not limit the vasodilator effect observed by a NO donor (a ruthenium complex) [47].

This work contributes to the understanding of the NO participation and association with contractile processes and tracheal hyper-responsiveness. Notably, we have shown that 100 μg/mL of AuNPs can induce hyperreactivity on the airways of both female and male rats. However, lower concentrations have not important biological effects, suggesting important observations for establishing biosafety margins in the potential use of these metallic nanoparticles. More details are needed to propose an action mechanism, as our research group has reported for other metallic nanoparticles in trachea rings. In this respect, Gonzalez et al. (2011) and Ramirez-Lee et al. (2014) determined the impact of 45 nm silver nanoparticles (AgNPs) (0.1–100 μg/mL) in the
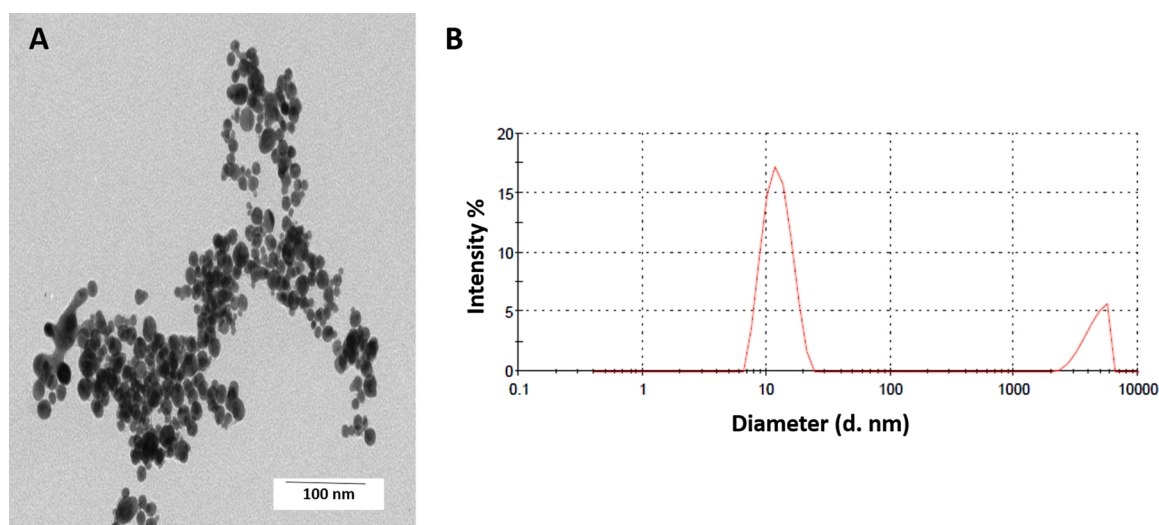

Fig. 1. AuNPs have spherical size, poly-disperse, and are stable. TEM micrographs showing the spherical shape of the AuNPs dispersed in water (A), the correspondent size distribution obtained by DLS (B).
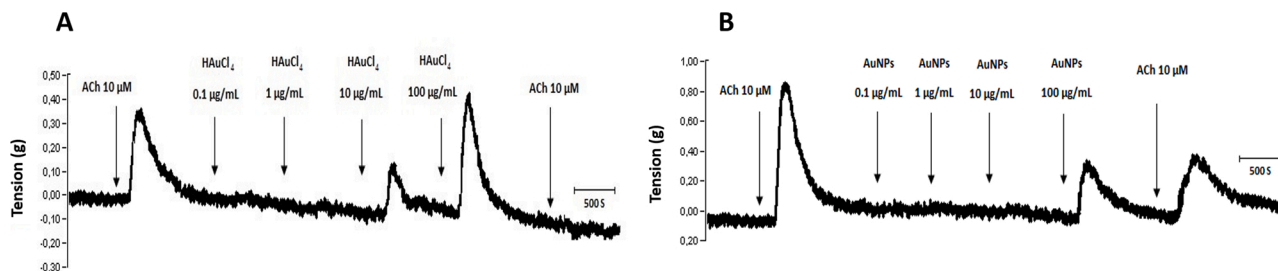
Fig. 2. Effect of cumulative concentrations of (A) HAuCl$_4$ and (B) AuNPs (0.1, 1.0, 10, and 100 μg/mL) on the muscle tone of isolated rings of male rat trachea, respectively. Representative trace of three independent experiments.
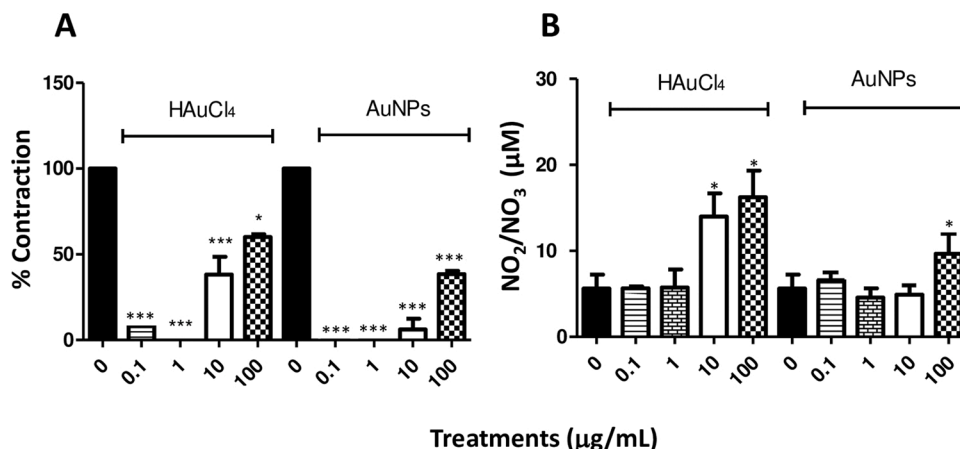

Fig. 3. (A) Comparing the percentage of contraction induced by HAuCl$_4$ and AuNPs (0.1, 1.0, 10 and 100 μg/mL), calculated as the % of the tension with respect to the 100 % contraction induced by 10 μg/mL ACh. (B) Basal NO production compared to NO production in the presence of HAuCl$_4$ and AuNPs (0.1, 1.0, 10 and 10 μg/mL) in isolated rings of male rat trachea. The values represent the mean $\pm$ SEM (n = 3). * P $<$ 0.05 and *** P $<$ 0.001 vs ACh control.
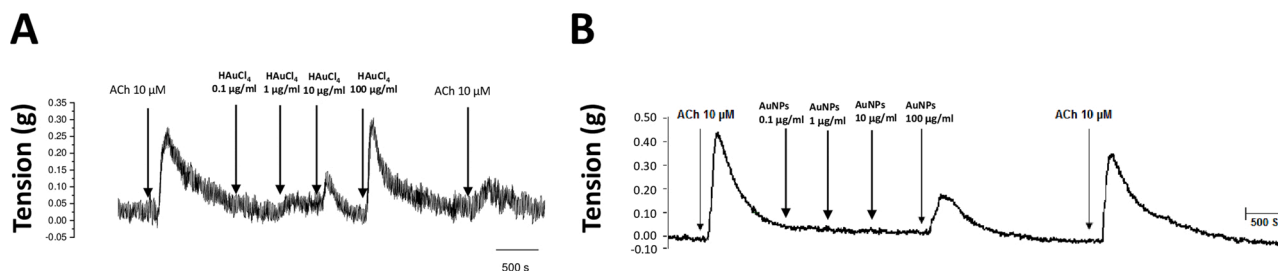

Fig. 4. Effect of cumulative concentrations of (A) HAuCl$_4$ and (B) AuNPs (0.1, 1.0, 10, and 100 μg/mL) on the muscle tone of isolated rings of female rat trachea, respectively. Representative trace of three independent experiments.

trachea, where the increment on the NO levels was possible to associate to the alteration of acetylcholine muscarin receptor [43,44].

3.3. AuNPs formation in a physiological solution containing HEPES

Interestingly, this work demonstrates that 1) there is no significant difference for the trachea isolated rings of male and female rat, and 2) the profile of effects on smooth muscle with both HAuCl$_4$ as ionization control and treatments with AuNPs are similar, as well as the possible mediator involved, NO (Fig. 5). Notably, pink to purplish physiological solutions were observed in chambers containing isolated trachea rings treated with HAuCl$_4$. The possible obtention of AuNPs in physiological solution could be an explanation of similar profile effects. Therefore, an additional experiment performed, adding HAuCl$_4$•3H$_2$O (100 μg/mL or 0.25 mM) to the physiological solution (HEPES 0, 5, 10, 15, and 20 mM) at pH 7.4 and 37 °C and monitorization by UV–vis (Jenway 7210). Final colloids showed pink to purplish colors (Fig. 6A), and UV–vis spectra

showed a signal of surface plasmon resonance at 557 nm corresponding to the AuNPs formation (Fig. 6B) TEM image exhibited spherical AuNPs with an average diameter of 22.7 $\pm$ 5.82 nm (Fig. 6C). Differences in colloidal colors indicate various particle sizes as the HEPES concentration increased, with hydrodynamic diameter from12.4–98.9 nm and average zeta potential of -27.0 $\pm$ 0.6. We observed some particles precipitated into the HEPES 5 mM and 20 mM solutions after 30 h. The formation of AuNP with HEPES for reducing and stabilizing nanoparticles reported in the literature. For instance, Xie et al. [48] reported that 20 mM HAuCl$_4$ and 100 mM HEPES (pH 7.4, 25 °C) achieved branched AuNPs (15–25 nm x 8 nm) after 30 min with a greenish-blue color colloid (surface plasmon resonance at 518 and 658 nm) [48]. Later, Chen et al. [49] synthesized spindle, octahedron, and decahedron AuNPs (20−50 nm) using 1:10, 1:20, 1:30, and 1:40 M ratios of HAuCl$_4$ (10 mmol/L)/HEPES (50 mmol/L) with pH 7.4 and at room temperature (surface plasmon resonance at 554 nm) [49]. Saverot et al. [50] obtained 30 nm branched AuNPs with 2 mM HAuCl$_4$•3H$_2$O and 150 mM
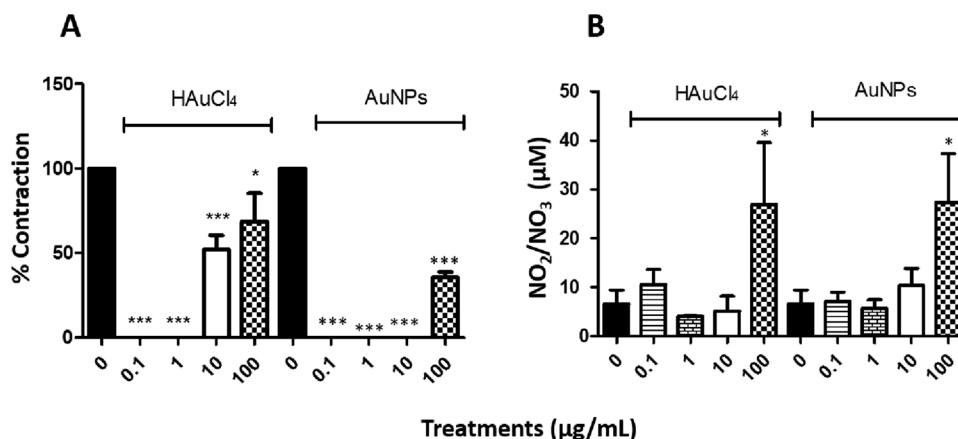
Fig. 5. (A) Percentage of contraction induced by HAuCl$_4$ and AuNPs (0.1 and 100 µg/mL), calculated as the % of the tension with respect to the 100 % contraction induced by 10 µg/mL ACh. (B) basal NO production compared to NO production in the presence of HAuCl$_4$ and AuNPs (0.1 and 100 µg/mL) in isolated rings of female rat trachea. The values represent the mean ± SEM (n = 3). * P < 0.05 and *** P < 0.001 vs ACh control.
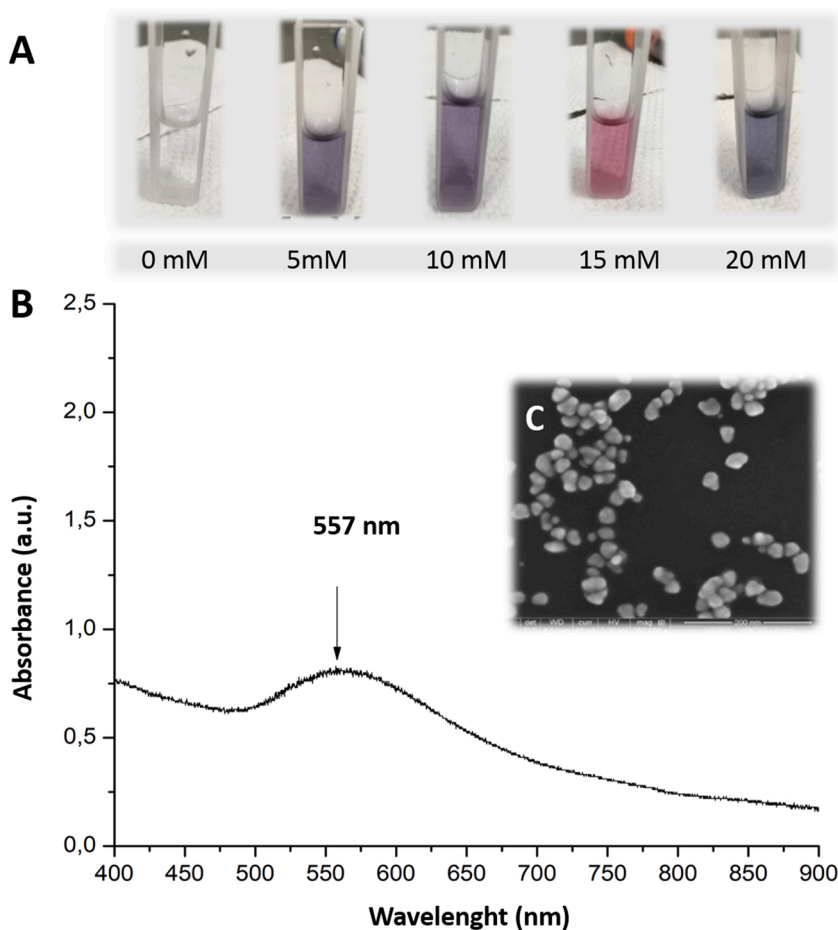

Fig. 6. AuNPs formation in physiological solution. (A) A 100 µg/mL solution of HAuCl$_4$ and five different concentrations of HEPES in the physiological solution were tested (0, 5, 10, 15, and 20 mM) at 37 °C and pH 7.4. Formation of AuNPs was observable after 30 min and remained after 24 h. (B) UV–vis spectra of AuNPs formed in the physiological solution with HEPES 20 mM (37 °C, pH 7.4), the normal concentration of HEPES used in *ex vivo* experiments with isolated rings. Maximum absorption at 557 nm indicates the surface resonance plasmon of AuNPs. (C) TEM micrograph of AuNPs formed in HEPES solution.

HEPES with pH 7.4 and at room temperature (surface plasmon resonance at 530 and 740 nm) [50]. Thus, the physiological buffer containing HEPES in our *ex vivo* experiments acted as a reducing medium for HAuCl$_4$•3H$_2$O and exerting similar results in trachea rings that those groups treated initially with spherical AuNPs. Further studies in our group are conducting in the synthesis and characterization of AuNPs formation in HEPES solution and its implications in physiological studies.

4. Conclusions

AuNPs induced similar transient contraction exerted by ACh only at the concentration of 100 µg/mL, but not in the concentration range of 0.1–10 µg/mL in isolated rings of male and female rat trachea. The contractile actions of these NPs and the potential mediator involved and identified was NO. Some of these effects were common and comparable with its ionization control, HAuCl$_4$•3H$_2$O, although to a different magnitude. Interestingly, it was observed that the cumulative

concentrations in the presence of HAuCl$_4$•3H$_2$O blocked the transient contractile effect induced by ACh at the end of this treatment, but not by AuNPs, a fact that could suggest a secondary or toxic effect promoted by this control. In the case of AuNPs, the results obtained in this study show that these NPs could confer a bio-inert character in a concentration range of 0.1−10 µg/mL, however from 100 µg/mL, they could trigger hyperresponsiveness of the airways. These aspects must be studied in greater detail to establish the margins of biosafety. Further evaluations on the effect of HAuCl$_4$ in *ex vivo* experiments with isolated tissues should be conducted since the formation of AuNPs in physiological buffers occur.

CRediT authorship contribution statement

Daniel Alberto Maldonado-Ortega: Investigation, Visualization, Writing - original draft, Data curation. **Gabriela Navarro-Tovar:** Writing - review & editing, Investigation, Visualization, Data curation. **Gabriel Martínez-Castañón:** Validation, Data curation. **Carmen Gonzalez:** Conceptualization, Writing - original draft, Supervision, Funding acquisition, Project administration, Investigation.

Declaration of Competing Interest

The authors declare no conflict of interest.

Acknowledgements

References

[1] M. Das, K.H. Shim, S.S.A. An, D.K. Yi, Review on gold nanoparticles and their applications, J. Toxicol. Environ. Health Sci. 3 (4) (2011) 193–205, https://doi.org/10.1007/s13530-011-0109-y.

[2] Nanoeffects in Ancient Technology and Art and in Space, In Fundamentals and Applications of Nano Silicon in Plasmonics and Fullerines Edited by Munir Nayfeh, Elsevier, 2018, pp. 497–518, https://doi.org/10.1016/b978-0-323-48057-4.00016-5.

[3] D.T. Thompson, Michael Faraday's recognition of Ruby Gold: the birth of modern nanotechnology, Gold Bull. 40 (4) (2008) 267–269, https://doi.org/10.1007/BF03215598.

[4] C. Daruich De Souza, B. Ribeiro Nogueira, M.E.C.M. Rostelato, Review of the methodologies used in the synthesis gold nanoparticles by chemical reduction, J. Alloys. Compd. 798 (2019) 714–740, https://doi.org/10.1016/j.jallcom.2019.05.153.

[5] J. Fan, Y. Cheng, M. Sun, Functionalized gold nanoparticles: synthesis, properties and biomedical applications, Chem. Rec. 20 (12) (2020) 1474–1504, https://doi.org/10.1002/tcr.202000087.

[6] C. Kohout, C. Santi, L. Polito, Anisotropic gold nanoparticles in biomedical applications, Int. J. Mol. Sci. 19 (11) (2018) 3385, https://doi.org/10.3390/ijms19113385.

[7] S. Anniebell, S.C.B. Gopinath, Polymer conjugated gold nanoparticles in biomedical applications, Curr. Med. Chem. 25 (12) (2018) 1433–1445, https://doi.org/10.2174/0929867324666170116123633.

[8] X. Chen, X. Zhao, G. Wang, Review on marine carbohydrate-based gold nanoparticles represented by alginate and chitosan for biomedical application, Carbohydr. Polym. 244 (2020), 116311, https://doi.org/10.1016/j.carbpol.2020.116311.

[9] R.F. de Araújo, A.A. de Araújo, J.B. Pessoa, F.P. Freire Neto, G.R. da Silva, A.L.C. S. Leitão Oliveira, T.G. de Carvalho, H.F.O. Silva, M. Eugênio, C. Sant'Anna, L.H. S. Gasparotto, Anti-inflammatory, analgesic and anti-tumor properties of gold nanoparticles, Pharmacol. Rep. 69 (1) (2017) 119–129, https://doi.org/10.1016/j.pharep.2016.09.017.

[10] M.A. Hamzawy, A.M. Abo-Youssef, H.F. Salem, S.A. Mohammed, Antitumor activity of intratracheal inhalation of temozolomide (TMZ) loaded into gold nanoparticles and/or liposomes against urethane-induced lung cancer in BALB/c mice, Drug Deliv. 24 (1) (2017) 599–607, https://doi.org/10.1080/10717544.2016.1247924.

[11] H. Horo, S. Bhattacharyya, B. Mandal, L.M. Kundu, Synthesis of functionalized silk-coated chitosan-gold nanoparticles and microparticles for target-directed delivery of antitumor agents, Carbohydr. Polym. (2021) 117659, https://doi.org/10.1016/j.carbpol.2021.117659.

[12] S. Tummala, M.N.S. Kumar, S.K. Pindiprolu, Improved anti-tumor activity of oxaliplatin by encapsulating in anti-DR5 targeted gold nanoparticles, Drug Deliv. 23 (9) (2016) 3505–3519, https://doi.org/10.1080/10717544.2016.1199606.

[13] A. Folorunso, S. Akintelu, A.K. Oyebamiji, S. Ajayi, B. Abiola, I. Abdusalam, A. Morakinyo, Biosynthesis, characterization and antimicrobial activity of gold nanoparticles from leaf extracts of Annona muricata, J. Nanostructure Chem. 9 (2) (2019) 111–117, https://doi.org/10.1007/s40097-019-0301-1.

[14] A. Rai, A. Prabhune, C.C. Perry, Antibiotic mediated of gold nanoparticles with potent antimicrobial activity and their application in antimicrobial coatings, J. Mater. Chem. 20 (32) (2010) 6789–6798, https://doi.org/10.1039/c0jm00817f.

[15] F.R. Souza, F. Fornasier, A.S. Carvalho, B.M. Silva, M.C. Lima, A.S. Pimentel, Polymer-coated gold nanoparticles and polymeric nanoparticles as nanocarrier of the BP100 antimicrobial peptide through a lung surfactant model, J. Mol. Liq. 314 (2020), 113661, https://doi.org/10.1016/j.molliq.2020.113661.

[16] T.G. de Carvalho, V.B. Garcia, A.A. de Araújo, L.H. da Silva Gasparotto, H. Silva, G. C.B. Guerra, E. de Castro Miguel, R.F. de Carvalho Leitão, D.V. da Silva Costa, L. J. Cruz, A.B. Chan, R.F. de Araújo Júnior, Spherical neutral gold nanoparticles improve anti-inflammatory response, oxidative stress and fibrosis in alcohol-methamphetamine-induced liver injury in rats, Int. J. Pharm. 548 (1) (2018) 1–14, https://doi.org/10.1016/j.ijpharm.2018.06.008.

[17] N.U. Islam, I. Khan, A. Rauf, N. Muhammad, M. Shahid, M.R. Shah, Antinociceptive, muscle relaxant and sedative activities of gold nanoparticles generated by methanolic extract of Euphorbia milii, BMC Complement. Altern. Med. 15 (1) (2015) 160, https://doi.org/10.1186/s12906-015-0691-7.

[18] H. Mahmoudvand, M. Khaksarian, K. Ebrahimi, S. Shiravand, S. Jahanbakhsh, M. Niazi, S. Nadri, Antinociceptive effects of green synthesized copper nanoparticles alone or in combination with morphine, Ann. Med. Surg. 51 (2020) 31–36, https://doi.org/10.1016/j.amsu.2019.12.006.

[19] C.M. Jewell, J.-M. Jung, P.U. Atukorale, R.P. Carney, F. Stellacci, D.J. Irvine, Oligonucleotide delivery by cell-penetrating "Striped" nanoparticles, Angew. Chem. Int. 50 (51) (2011) 12312–12315, https://doi.org/10.1002/anie.201104514.

[20] J.H. Kim, J.H. Yeom, J.J. Ko, M.S. Han, K. Lee, S.Y. Na, J. Bae, Effective delivery of anti-miRNA DNA oligonucleotides by functionalized gold nanoparticles, J. Biotechnol. 155 (3) (2011) 287–292, https://doi.org/10.1016/j.jbiotec.2011.07.014.

[21] Domènech Trigueros, Marfany Toulis, In vitro gene delivery in retinal pigment epithelium cells by plasmid DNA-Wrapped gold nanoparticles, Genes 10 (4) (2019) 289, https://doi.org/10.3390/genes10040289.

[22] L.A. Dykman, S.A. Staroverov, P.V. Mezhenny, A.S. Fomin, S.V. Kozlov, A. A. Volkov, V.N. Laskavy, S.Y. Shchyogolev, Use of a synthetic foot-and-mouth disease virus peptide conjugated to gold nanoparticles for enhancing immunological response, Gold Bull. 48 (1–2) (2015) 93–101, https://doi.org/10.1007/s13404-015-0165-1.

[23] H.W. Kao, Y.Y. Lin, C.C. Chen, K.H. Chi, D.C. Tien, C.C. Hsia, W.J. Lin, F.Du Chen, M.H. Lin, H.E. Wang, Biological characterization of cetuximab-conjugated gold nanoparticles in a tumor animal model, Nanotechnology 25 (29) (2014), 295102, https://doi.org/10.1088/0957-4484/25/29/295102.

[24] M. Schäffler, F. Sousa, A. Wenk, L. Sitia, S. Hirn, C. Schleh, N. Haberl, M. Violatto, M. Canovi, P. Andreozzi, M. Salmona, P. Bigini, W.G. Kreyling, S. Krol, Blood protein coating of gold nanoparticles as potential tool for organ targeting, Biomaterials 35 (10) (2014) 3455–3466, https://doi.org/10.1016/j.biomaterials.2013.12.100.

[25] H. Sekimukai, N. Iwata-Yoshikawa, S. Fukushi, H. Tani, M. Kataoka, T. Suzuki, H. Hasegawa, K. Niikura, K. Arai, N. Nagata, Gold nanoparticle-adjuvanted S protein induces a strong antigen-specific IgG response against severe acute respiratory syndrome-related coronavirus infection, but fails to induce protective antibodies and limit eosinophilic infiltration in lungs, Microbiol. Immunol. 64 (1) (2020) 33–51, https://doi.org/10.1111/1348-0421.12754.

[26] H. Nekounam, Z. Allahyari, S. Gholizadeh, E. Mirzaei, M.A. Shokrgozar, R. Faridi-Majidi, Simple and robust fabrication and characterization of conductive carbonized nanofibers loaded with gold nanoparticles for bone tissue engineering applications, bioRxiv (2020), https://doi.org/10.1101/2020.03.28.013383, p. 2020.03.28.013383.

[27] M. Shevach, B.M. Maoz, R. Feiner, A. Shapira, T. Dvir, Nanoengineering gold particle composite fibers for cardiac tissue engineering, J. Mater. Chem. B 1 (39) (2013) 5210–5217, https://doi.org/10.1039/c3tb20584c.

[28] V. Mazeiko, A. Kausaite-Minkstimiene, A. Ramanaviciene, Z. Balevicius, A. Ramanavicius, Gold nanoparticle and conducting polymer-polyaniline-based nanocomposites for glucose biosensor design, Sensors Actuat., B-Chem. 189 (2013) 187–193, https://doi.org/10.1016/j.snb.2013.03.140.

[29] Y. Wang, E.C. Alocilja, Gold nanoparticle-labeled biosensor for rapid and sensitive detection of bacterial pathogens, J. Biol. Eng. 9 (1) (2015) 16, https://doi.org/10.1186/s13036-015-0014-z.

[30] L. Zheng, G. Cai, S. Wang, M. Liao, Y. Li, J. Lin, A microfluidic colorimetric biosensor for rapid detection of Escherichia coli O157:H7 using gold nanoparticle aggregation and smart phone imaging, Biosens. Bioelectron. 124–125 (2019) 143–149, https://doi.org/10.1016/j.bios.2018.10.006.

[31] G. Chauhan, V. Chopra, A. Tyagi, G. Rath, R.K. Sharma, A.K. Goyal, Gold nanoparticles composite-folic acid conjugated graphene oxide nanohybrids" for targeted chemo-thermal cancer ablation: in vitro screening and in vivo studies, Eur. J. Pharm. Sci. 96 (2017) 351–361, https://doi.org/10.1016/j.ejps.2016.10.011.

[32] J. Park, S. Pramanick, J. Kim, J. Lee, W.J. Kim, Nitric oxide-activatable gold nanoparticles for specific targeting and photo-thermal ablation of macrophages, Chem. Commun. 53 (81) (2017) 11229–11232, https://doi.org/10.1039/c7cc06420a.

[33] H.B. Ruttala, T. Ramasamy, B.K. Poudel, R.R.T. Ruttala, S.G. Jin, H.G. Choi, S. K. Ku, C.S. Yong, J.O. Kim, Multi-responsive albumin-lonidamine conjugated hybridized gold nanoparticle as a combined photothermal-chemotherapy for synergistic tumor ablation, Acta Biomater. 101 (2020) 531–543, https://doi.org/10.1016/j.actbio.2019.11.003.

[34] J.K. Kang, J.C. Kim, Y. Shin, S.M. Han, W.R. Won, J. Her, J.Y. Park, K.T. Oh, Principles and applications of nanomaterial-based hyperthermia in cancer therapy, Arch. Pharmacal. Res 43 (1) (2020) 46–57, https://doi.org/10.1007/s12272-020-01206-5.

[35] M. Pretze, V. von Kiedrowski, R. Runge, R. Freudenberg, R. Hübner, G. Davarci, R. Schirrmacher, C. Wängler, B. Wängler, αvβ3-specific gold nanoparticles for fluorescence imaging of tumor angiogenesis, Nanomaterials 11 (1) (2021) 1–30, https://doi.org/10.3390/nano11010138.

[36] X. Ma, Y. Wu, S. Jin, Y. Tian, X. Zhang, Y. Zhao, L. Yu, X.J. Liang, Gold nanoparticles induce autophagosome accumulation through size-dependent nanoparticle uptake and lysosome impairment, ACS Nano 5 (11) (2011) 8629–8639, https://doi.org/10.1021/nn202155y.

[37] C. Freese, C. Uboldi, M.I. Gibson, R.E. Unger, B.B. Weksler, I.A. Romero, P. O. Couraud, C.J. Kirkpatrick, Uptake and cytotoxicity of citrate-coated gold nanospheres: Comparative studies on human endothelial and epithelial cells, Part. Fibre Toxicol. 9 (1) (2012) 23, https://doi.org/10.1186/1743-8977-9-23.

[38] M. Bhamidipati, L. Fabris, Multiparametric assessment of gold nanoparticle cytotoxicity in cancerous and healthy cells: the role of size, shape, and surface chemistry, Bioconjugate Chem. 28 (2) (2017) 449–460, https://doi.org/10.1021/acs.bioconjchem.6b00605.

[39] X.D. Zhang, D. Wu, X. Shen, P.X. Liu, N. Yang, B. Zhao, H. Zhang, Y.M. Sun, L. A. Zhang, F.Y. Fan, Size-dependent in vivo toxicity of PEG-coated gold nanoparticles, Int. J. Nanomed. Nanosurg. 6 (2011) 2071–2081, https://doi.org/10.2147/ijn.s21657.

[40] A.L. Bailly, F. Correard, A. Popov, G. Tselikov, F. Chaspoul, R. Appay, A. Al-Kattan, A.V. Kabashin, D. Braguer, M.A. Esteve, In vivo evaluation of safety, biodistribution and pharmacokinetics of laser-synthesized gold nanoparticles, Sci. Rep. 9 (1) (2019) 1–12, https://doi.org/10.1038/s41598-019-48748-3.

[41] N.A. Holland, L.C. Thompson, A.K. Vidanapathirana, R.N. Urankar, R.M. Lust, T. R. Fennell, C.J. Wingard, Impact of pulmonary exposure to gold core silver nanoparticles of different size and capping agents on cardiovascular injury, Part. Fibre Toxicol. 13 (1) (2016), https://doi.org/10.1186/S12989-016-0159-Z.

[42] A.M. Alkilany, A. Shatanawi, T. Kurtz, R.B. Caldwell, R.W. Caldwell, Toxicity and cellular uptake of gold nanorods in vascular endothelium and smooth muscles of isolated rat blood vessel: importance of surface modification, Small 8 (8) (2012) 1270–1278, https://doi.org/10.1002/smll.201101948.

[43] C. González, S. Salazar-García, G. Palestino, P.P. Martínez-Cuevas, M.A. Ramírez-Lee, B.B. Jurado-Manzano, H. Rosas-Hernández, N. Gaytán-Pacheco, G. Martel, R. Espinosa-Tanguma, A.S. Biris, S.F. Ali, Effect of 45nm silver nanoparticles (AgNPs) upon the smooth muscle of rat trachea: role of nitric oxide, Toxicol. Lett. 207 (3) (2011) 306–313, https://doi.org/10.1016/j.toxlet.2011.09.024.

[44] M.A. Ramírez-Lee, H. Rosas-Hernández, S. Salazar-García, J.M. Gutiérrez-Hernández, R. Espinosa-Tanguma, F.J. González, S.F. Ali, C. González, Silver nanoparticles induce anti-proliferative effects on airway smooth muscle cells. Role of nitric oxide and muscarinic receptor signaling pathway, Toxicol. Lett. 224 (2) (2014) 246–256, https://doi.org/10.1016/j.toxlet.2013.10.027.

[45] S.A. Moreno-Álvarez, G.A. Martínez-Castañón, N. Niño-Martínez, J.F. Reyes-Macías, N. Patiño-Marín, J.P. Loyola-Rodríguez, F. Ruiz, Preparation and bactericide activity of gallic acid stabilized gold nanoparticles, J. Nanopart. Res. 12 (8) (2010) 2741–2746, https://doi.org/10.1007/s11051-010-0060-x.

[46] H. Rosas-Hernández, S. Jiménez-Badillo, P.P. Martínez-Cuevas, E. Gracia-Espino, H. Terrones, M. Terrones, S.M. Hussain, S.F. Ali, C. González, Effects of 45-nm silver nanoparticles on coronary endothelial cells and isolated rat aortic rings, Toxicol. Lett. 191 (2–3) (2009) 305–313, https://doi.org/10.1016/j.toxlet.2009.09.014.

[47] B.R. Silva, C.N. Lunardi, K. Araki, J.C. Biazzotto, R.S. Da Silva, L.M. Bendhack, Gold nanoparticle modifies nitric oxide release and vasodilation in rat aorta, J. Chem. Biol. 7 (2) (2014) 57–65, https://doi.org/10.1007/s12154-014-0109-x.

[48] J. Xie, J.Y. Lee, D.I.C. Wang, Seedless, surfactantless, high-yield synthesis of branched gold nanocrystals in HEPES buffer solution, Chem. Mater. 19 (11) (2007) 2823–2830, https://doi.org/10.1021/cm0700100.

[49] R. Chen, J. Wu, H. Li, G. Cheng, Z. Lu, C.M. Che, Fabrication of gold nanoparticles with different morphologies in HEPES buffer, Rare Met. 29 (2) (2010) 180–186, https://doi.org/10.1007/s12598-010-0031-5.

[50] S. Saverot, X. Geng, W. Leng, P.J. Vikesland, T.Z. Grove, L.R. Bickford, Facile, tunable, and SERS-enhanced HEPES gold nanostars, RSC Adv. 6 (35) (2016) 29669–29673, https://doi.org/10.1039/C6RA00450D.